
Application of Linear Filter and Moment Equation for Parametric Rolling in Irregular Longitudinal Waves

Yuuki Maruyama · Atsuo Maki · Leo Dostal · Naoya Umeda

Received: date / Accepted: date

Abstract Parametric rolling is one of the dangerous dynamic phenomena. In order to discuss the safety of a vessel when a dangerous phenomenon occurs, it is important to estimate the probability of certain dynamical behavior of the ship with respect to a certain threshold level. In this paper, the moment values are obtained by solving the moment equations. Since the stochastic differential equation(SDE) is needed to obtain the moment equations, the Autoregressive Moving Average(ARMA) filter is used. The effective wave is modeled by using the 6th-order ARMA filter. In addition, the parametric excitation process is modeled by using a non-memory transformation obtained from the relationship between GM and wave elevation. The resulting system of equations is represented by the 8th-order Itô stochastic differential equation, which consists of a second-order SDE for the ship motion and a 6th-order SDE for the effective wave. This system has nonlinear components. Therefore, the cumulant neglect closure method is used as higher-order moments need to be truncated. Furthermore, the probability density function of roll angle is determined by using moment values obtained from the SDE and the moment equation. Here, two types of the probability density function are suggested and have a good agreement.

Keywords Parametric Rolling · Moment Equation · Stochastic Differential Equation · Cumulant Neglect · Linear Filter

Yuuki Maruyama · Atsuo Maki · Naoya Umeda
Department of Naval Architecture and Ocean Engineering, Graduate School of Engineering, Osaka University, 2-1 Yamadaoka, Suita, Osaka, Japan
E-mail: yuuki_maruyama@naoe.eng.osaka-u.ac.jp

Leo Dostal
Institute of Mechanics and Ocean Engineering, Hamburg University of Technology, 21043 Hamburg, Germany

1 Introduction

When roll motion in irregular waves is considered in the framework of the stochastic theory, the irregular excitation due to waves is assumed as a stochastic process. However, the real noise such as the processes of wind or sea waves are not of white noise type but of colored noise type. Therefore, a real noise process for sea waves should be generated from filtered white-noise via the stochastic differential equation (SDE) [1]. From such a point of view, Spanos [2,3], Flower [4,5], and Thampi [6] applied earlier a linear filter for the generation of stochastic time series based on wave spectra (Pierson-Moskowitz wave spectrum and JONSWAP spectrum) using the ARMA process, which was a good approximation of the process obtained from sea wave spectra. Furthermore, Degtyarev and Reed [7] and Degtyarev and Gankevich [8] discussed the autoregressive moving average model, which was used to describe the wave surface and incident random waves. On the other hand, concerning wind process generation, Nichita [9], Dostal et al. [10], and Maki et al. [11] also utilized liner filters for white noise.

Parametric rolling is a roll motion that is induced by the periodic variation of the restoring moment and tends to occur when the natural roll frequency is about twice the encounter frequency of ocean waves. This variation is caused by the change in the area of the water plane around the ship hull. Many studies have been conducted on parametric rolling [12, 13, 14, 15, 16] and it was shown that Parametric rolling is related to container loss accidents. For preventing container loss accidents, the second-generation intact stability criteria developed by the International Maritime Organization (IMO) could be utilized [17]. With respect to parametric rolling, the sub-committee on ship design and construction of the IMO reported that the uncoupled roll model based on the Froude-Krylov assumption generally provides more conservative estimates [18]. The new criteria in its di-

rect stability assessment require stochastically limiting the roll angle below the threshold values by means of the direct counting method, which is a kind of the Monte Carlo simulation (MCS). However, such simulation is highly time-consuming. Therefore, a theoretical estimation method is highly desirable as a preliminary tool.

In order to discuss the safety of a vessel when a dangerous phenomenon occurs, it is important to estimate the probability of certain dynamical behavior of the ship with respect to a certain threshold level. For this purpose, it is desirable to analytically or theoretically obtain a probability density function (PDF) of a critical dynamical response. One of the candidates to theoretically obtain the PDF in a nonlinear system is to solve the Fokker-Planck-Kolmogorov (FPK) equation analytically [19]. Unfortunately, the application of this method is slightly limited to simple low dimensional nonlinear systems driven by white noise, such that the direct application of this method to the problem of parametric roll motion driven by colored noise is not possible. In order to approach such problems the equivalent linearization method was developed [20, 21], which approximates a nonlinear system using linear components. One of the successive method to solve the FPK equation for this parametric rolling problem is the stochastic averaging method [22, 23, 24]. In this approach, the FPK equation for the averaged system is analytically solved. On the other hand, another method is to use moment equations [25, 26]. In the case of using higher-order moment equations, a nonlinear effect can be reflected in the analysis. In Naval Architecture, Nekrasov [27] investigated the moment method for the ship motion. If the system is linear, the response is a Gaussian process and the transfer function can be used. Therefore, it is easy to obtain an accurate PDF. As is well known, the response for a strong nonlinear system has a non-Gaussian distribution [28]. In the case of the parametric rolling problem, the PDF of roll angle is not Gaussian as pointed out by Belenky [29]. With respect to modelling the PDF, Mohamad et al. [30] and Maki [31] determined the shape of the non-Gaussian PDF. So far, some researches use a combination of moment equations and a linear filter, which has been applied in the field of naval architecture and ocean engineering. For example, Francescutto and Naito [32] and Su et al. [33] considered the roll motion in beam seas using a 4th-order linear filter and a moment equation. Chai et al. [34] analyzed the response of parametric rolling in irregular waves by using Monte Carlo simulation (MCS). Dostal et al. [1] used the Local Statistical Linearization in combination with moment equations. So far, there has been little research on combining the moment equations including a non-Gaussian process and the non-Gaussian PDF of roll angle.

In this study, the variation of metacentric height (GM) is modeled by using the ARMA filter and the non-memory transformation. Then the results are examined by compari-

son with the result obtained by using the superposition principle. The objective of this paper is to obtain the moment values by solving the moment equations and determine the parameter of the roll angle's PDF based on these moment values and the predefined PDF shape. Thus, this paper is concerned with the moment equation derived from the SDE representing the ship motion and the ocean wave elevation. Thereby, the PDF of the roll angle is determined by using stochastic moments. By this means, two types of PDF are chosen and their coefficients are optimized.

2 Linear filter

When a stochastic differential equation (SDE) is used to model parametric rolling, then it is common to model the parametric excitation process as a stationary random process with zero mean [1][22]. It is generally acceptable that a parametric excitation (real noise) itself, calculated on the basis of hydrodynamic assumptions, is regarded as a stochastic process. However, an Itô stochastic differential equation, which uses a driving noise derived from white noise, is needed in order to determine moment equations. Therefore it is appropriate to represent the parametric excitation process approximately by a stochastic differential equation. In this study, as a means of approximating real noise from white noise, the time series of the effective wave is modeled using an ARMA process.

In this study, the ITTC spectrum is used as the ocean wave spectrum, which is given by

$$S_w(\omega) = \frac{173H_{1/3}^2}{T_{01}^4\omega^5} \exp\left(-\frac{691}{T_{01}^4\omega^4}\right) \quad (1)$$

Here, T_{01} and $H_{1/3}$ are the wave mean period and the significant wave height, respectively. In this study, the GM variation is calculated by applying the concept of Grim's effective wave[35] to irregular waves. The transfer function H_ζ which is necessary to obtain the effective wave spectrum S_{eff} , can be represented as in the following equation[36]:

$$H_\zeta(\omega, \chi) = H_{\zeta_c}(\omega, \chi) + iH_{\zeta_s}(\omega, \chi)$$

$$\begin{cases} H_{\zeta_c}(\omega, \chi) = \frac{\frac{\omega^2 L}{g} \cos \chi \sin\left(\frac{\omega^2 L}{2g} \cos \chi\right)}{\pi^2 - \left(\frac{\omega^2 L}{2g} \cos \chi\right)^2} \\ H_{\zeta_s}(\omega, \chi) = 0 \end{cases} \quad (2)$$

Here, ω denotes the wave angular frequency, χ denotes the heading angle from wave direction, g denotes gravitational

acceleration, and L denotes the wave length. With the use of this transfer function, the spectrum of the effective wave can be obtained as follows:

$$S_{\text{eff}}(\omega) = \left| H_{\zeta}(\omega) \right|^2 S_w(\omega) \quad (3)$$

If the ship is moving with the ship speed U , the frequency of wave encounter ω_e in deep water is given by [22] as follows:

$$\omega_e = \omega - \frac{\omega^2}{g} U \cos \chi. \quad (4)$$

Then, the spectrum with respect to the encounter frequency can be obtained as follows:

$$S(\omega_e) = S(\omega) \left| \frac{d\omega}{d\omega_e} \right|. \quad (5)$$

Here, $|d\omega/d\omega_e|$ can be calculated as

$$\left| \frac{d\omega}{d\omega_e} \right| = \left| \frac{1}{\sqrt{1 - \frac{4U\omega_e \cos \chi}{g}}} \right|. \quad (6)$$

Therefore, the effective wave spectrum for the case of a ship with the velocity U can be derived from Eqs.(3) and (5).

A higher-order linear filter is used to increase the parameters in the linear filter. Thereby, compared with a lower-order linear filter, a more accurate approximation can be expected to be obtained. The comparisons of 2nd, 4th, and 6th-order ARMA filter are shown in Appendix1. In this study, the following 6th-order ARMA filter is used:

$$x_1^{(6)} + \alpha_1 x_1^{(5)} + \alpha_2 x_1^{(4)} + \alpha_3 x_1''' + \alpha_4 x_1'' + \alpha_5 x_1' + \alpha_6 x_1 = k\sqrt{\pi}\{W'\}''' \quad (7)$$

This expression is rewritten as:

$$\begin{cases} \frac{dx_1}{dt} = x_2 - \alpha_1 x_1 \\ \frac{dx_2}{dt} = x_3 - \alpha_2 x_1 \\ \frac{dx_3}{dt} = x_4 - \alpha_3 x_1 + k\sqrt{\pi} \frac{dW(t)}{dt} \\ \frac{dx_4}{dt} = x_5 - \alpha_4 x_1 \\ \frac{dx_5}{dt} = x_6 - \alpha_5 x_1 \\ \frac{dx_6}{dt} = -\alpha_6 x_1 \end{cases} \quad (8)$$

Here, W denotes the standard Wiener process, and the notation for differentiation is represented by Lagrange's notation. As discussed later, the coefficients $\alpha_i (i = 1, \dots, 6)$ and

k are determined such that they agree with the effective wave spectrum. The transfer function $H_6(s)$ of the 6th-order linear filter is obtained from Eq. (8) as follows.

$$H_6(s) = \frac{ks^3\sqrt{\pi}}{s^6 + s^5\alpha_1 + s^4\alpha_2 + s^3\alpha_3 + s^2\alpha_4 + s\alpha_5 + \alpha_6} \quad (9)$$

Finally, the spectrum of the 6th-order ARMA process can be obtained as:

$$S_6(\omega) = 2|H_6(\omega)|^2 \frac{1}{2\pi} = \frac{k^2\omega^6}{(-\omega^6 + \alpha_2\omega^4 - \alpha_4\omega^2 + \alpha_6)^2 + (\alpha_1\omega^5 - \alpha_3\omega^3 + \alpha_5\omega)^2} \quad (10)$$

Next, it is necessary to obtain the coefficients $\alpha_i (i = 1, \dots, 6)$ and k of the ARMA process spectrum included in Eq. (10) such that they well fit the effective wave spectrum at a given T_{01} and $H_{1/3}$. It should be noted that even if these spectra have a good agreement, the system represented by Eq. (10) can become unstable and problems in the modeling of time series may occur. Therefore, in this study, the stability criterion of the corresponding system is added as one of the conditions to determine the coefficients of the linear filter. The algebraic equation used for the stability criterion is given by Eq. (11).

$$x^6 + \alpha_1 x^5 + \alpha_2 x^4 + \alpha_3 x^3 + \alpha_4 x^2 + \alpha_5 x + \alpha_6 = 0 \quad (11)$$

If all the real parts of the poles of Eq. (11) are negative, then the system is stable.

The computation results are shown in Table1 and Fig. 1. The solutions of Eq. (11) are obtained as $-0.0861 \pm 0.432i$, $-0.237 \pm 0.422i$, and $-0.0909 \pm 0.547i$. Since all real parts of these solutions are negative, it is clear that this system using the values from Table 1 is stable. In Fig. 1 it is observed that the 6th-order ARMA process spectrum agrees with the effective wave spectrum in the range $\omega = 0.3$ to 0.6 . However, in the range $\omega = 0.6$ to 0.8 , there is a discrepancy between S_6 and S_{eff} . Also, the time series of the effective wave is modelled by two methods. One is the method to solve numerically the stochastic differential equation (SDE) derived from Eq. (8) using Euler-Maruyama's method [37]. The other uses the inverse Fourier transformation as given in the following equation.

$$\zeta_w(t) = \sum_{n=1}^N \sqrt{2S_w(\omega_n)\Delta\omega_n} \cos(\omega_n t + \delta_n) \quad (12)$$

Here, ζ_w , $\Delta\omega_n$ and δ_n denote the wave elevation, the frequency interval, and the phase of the wave, respectively. Thereby, a method is used, which divides the frequency increments of the spectrum such that corresponding wave energies are equal to each other [38]. In this study, the latter is

called ‘‘superposition principle’’. Fig. 2 shows examples of time series which are obtained from the superposition principle and by solving the SDE from Eq. (8). In Fig. 1, the spectrum S_{SDE} of the time series using the linear filter overlaps the ARMA spectrum S_6 . Furthermore, Fig.3 shows that the PDF obtained solving the SDE agrees with the PDF obtained from the superposition result. Therefore, it is clear that the time series of the effective wave can be modeled sufficiently by using the linear filter. In Table 2, the statistical properties of the effective wave time series can be observed. In general, the value of Gaussian distribution’s kurtosis is defined as zero or three. In this study, this value is set to three. It is clear from Table 2 that the PDFs obtained solving the SDE and from the superposition result are a Gaussian distribution.

Table 1: Coefficients of Eq.(10)

Coefficient	ARMA6
α_1	0.828
α_2	0.935
α_3	0.424
α_4	0.227
α_5	0.0490
α_6	0.0140
k	0.0459

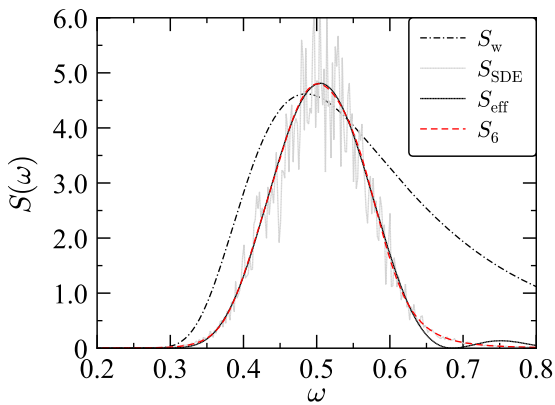


Fig. 1: Comparison among ITTC spectrum : S_w , spectrum of effective wave represented by Eq.(3) : S_{eff} , 6th-order ARMA spectrum : S_6 , and spectrum analysis result of time series obtained by solving SDE : S_{SDE} , sea state with $T_{01} = 9.99[s]$ and $H_{1/3} = 5.0[m]$

The process modelled using the ARMA filter is a Gaussian process. However, the parametric excitation process is

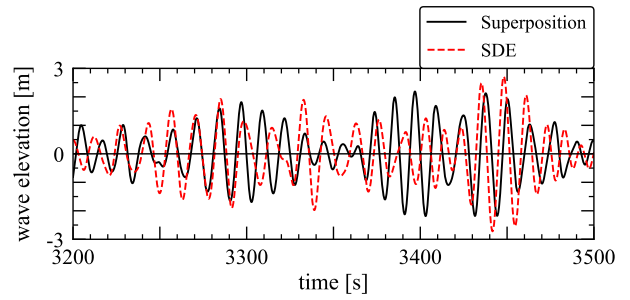


Fig. 2: Comparison of time series of effective wave between numerical simulation by superposition methodology : Superposition and result obtained by solving SDE : SDE, sea state with $T_{01} = 9.99[s]$ and $H_{1/3} = 5.0[m]$

Table 2: Statistical properties of effective wave’s time series

	Superposition	SDE
mean	7.10×10^{-6}	-1.54×10^{-5}
variance	0.792	0.796
skewness	2.32×10^{-4}	-1.64×10^{-5}
kurtosis	3.00	3.00

a non-Gaussian process. To generate the non-Gaussian process, the ARMA filter and the non-memory transformation are combined in this study. The role of the non-memory transformation is to translate a Gaussian process into a non-Gaussian process. In this study, this transformation is obtained from the relationship between the value of GM variation ΔGM and the wave elevation at amidship. We explain how to obtain the values of GM variation with an arbitrary wave elevation as follows. The restoring arm is calculated from hydrodynamic theory [39,40] using a wavelength which is the same as the ship length. Here, this restoring arm is obtained when the ship is heeling by two degrees in a regular wave. Then the wave crest or trough is set to be located at amidship, and GM is calculated for each wave elevation. As a result, the relationship between the amount of GM variation and the wave elevation at amidship can be obtained as shown in Fig. 4. Here, the wave elevation is positive when the wave trough is located at amidship, and the wave elevation is negative when the wave crest is located at amidship. In this study, the actual data is approximated by means of a 12th-order polynomial as Eq.(19). It can be observed in Fig. 4 that this approximation agrees with the actual data in all range.

The time series of the GM variation is generated by using the time series of an effective wave and the relationship in Fig. 4. Fig. 5 shows an example of time series of GM variation. In this figure, the black solid line shows the time series obtained by using the wave superposition principle

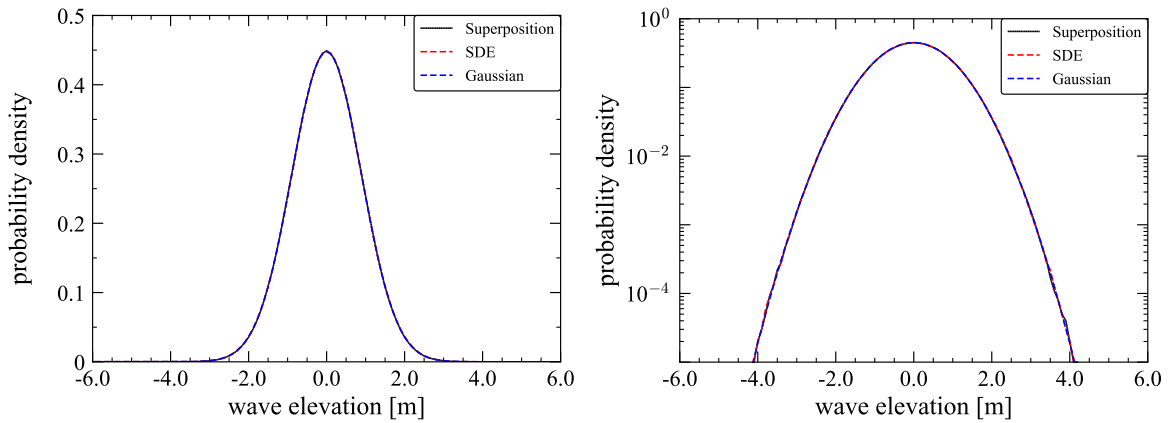


Fig. 3: Comparison of PDF of effective wave elevation among numerical simulation by superposition methodology : Superposition, result obtained by solving SDE : SDE, and Gaussian distribution by using moment equation result(Table5) : Gaussian, sea state with $T_{01} = 9.99[s]$ and $H_{1/3} = 5.0[m]$

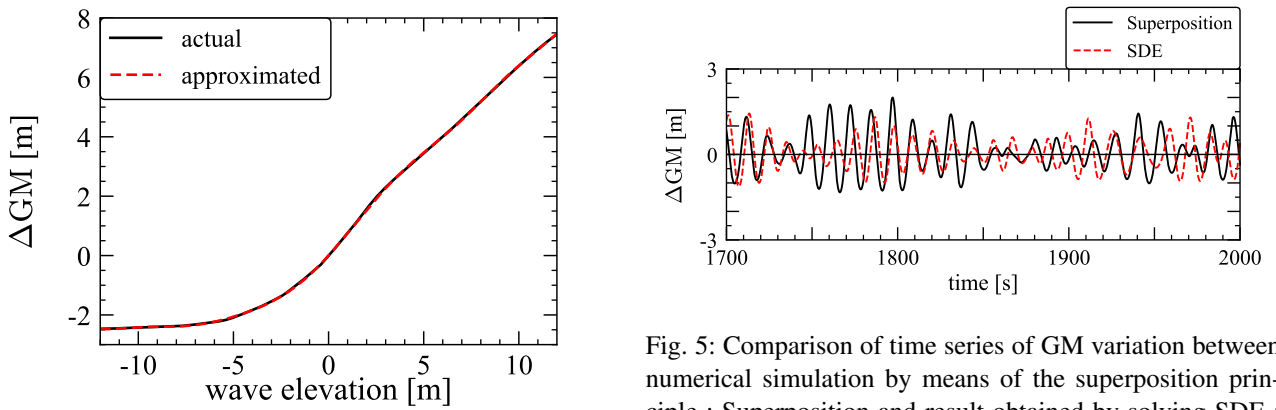


Fig. 4: Relationship between ΔGM and wave elevation at amidship, subject ship : C11

and the relationship in Fig. 4. The red solid line shows the time series from the result obtained by solving the stochastic differential equation derived from Eq. (8) and the relationship in Fig. 4. Also, Fig. 6 shows the PDFs of GM variation. The PDF obtained using the superposition principle matches everywhere with the PDF obtained by computing the SDE. The agreement of the peaks in the left panel of Fig. 6 and the tails in the right panel of Fig. 6, respectively, can be clearly observed. Fig. 7 shows the spectra of GM variation, where the spectrum obtained from the superposition principle overlaps the spectrum obtained by computing the SDE from (8). Therefore, it is clear that the time series of GM variation can be modeled sufficiently by using the linear filter and the relationship in Fig. 4.

Fig. 5: Comparison of time series of GM variation between numerical simulation by means of the superposition principle : Superposition and result obtained by solving SDE : SDE, sea state with $T_{01} = 9.99[s]$ and $H_{1/3} = 5.0[m]$

3 Moment Equation

For phenomena induced by irregular external excitation, this external excitation process is modeled as Gaussian random process in many studies. This is because the distribution of this random process has generally a close shape to a Gaussian distribution and a statistical analysis becomes feasible. However, some of the phenomena induced by irregular excitation have a non-Gaussian distribution [28]. The parametric rolling focused on in this study results from ship motion induced by irregular excitation. This phenomenon is a case which is non-Gaussian [29]. The purpose of this paper is to determine the probability density function of roll angle, based on the moment values obtained by determining the moment equations. In order to obtain the moment equations, the system of the ship motion needs to be represented by a stochastic differential equation (SDE) [41].

The procedure for deriving the moment equations from the SDE is explained in the following. The Itô SDE is repre-

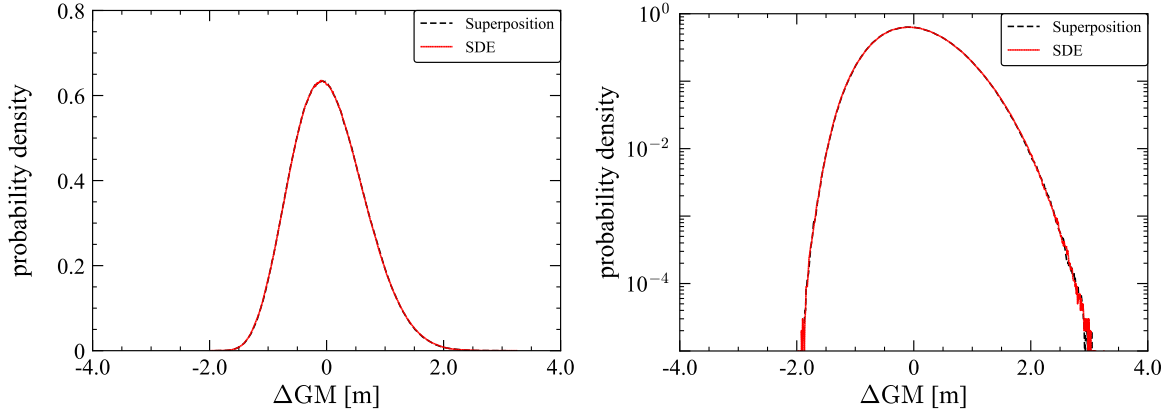


Fig. 6: Comparison of PDF of GM variation between numerical simulation by means of the superposition principle : Superposition and result obtained by solving : SDE, sea state with $T_{01} = 9.99[s]$ and $H_{1/3} = 5.0[m]$

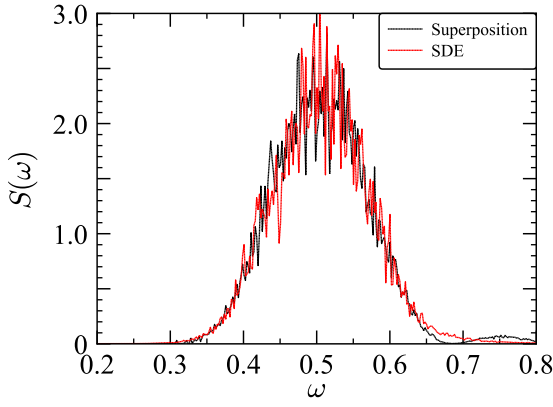


Fig. 7: Comparison of spectrum analysis results using time series from numerical simulation by means of the superposition principle : Superposition and time series obtained by solving SDE and using the relationship in Fig. 4) : SDE, sea state with $T_{01} = 9.99[s]$ and $H_{1/3} = 5.0[m]$

sented by

$$d\mathbf{X}(t) = \mathbf{a}(t)dt + \mathbf{b}(t)d\mathbf{W}(t), \quad (13)$$

where

$$\mathbf{X}(t) = \begin{pmatrix} X_1(t) \\ X_2(t) \\ \vdots \\ X_i(t) \end{pmatrix}, \mathbf{a}(t) = \begin{pmatrix} a_1(t) \\ a_2(t) \\ \vdots \\ a_i(t) \end{pmatrix}, \quad (14)$$

$$\mathbf{b}(t) = \begin{pmatrix} b_{11} & \cdots & b_{1j} \\ \vdots & \ddots & \vdots \\ b_{i1} & \cdots & b_{ij} \end{pmatrix}, \mathbf{W}(t) = \begin{pmatrix} W_1(t) \\ W_2(t) \\ \vdots \\ W_j(t) \end{pmatrix}.$$

Here, $\mathbf{a}(t)$ is the drift term and $\mathbf{b}(t)$ is the diffusion term. Moreover, $d\mathbf{W}(t)$ are independent increments of the standard Wiener process, whereby $d\mathbf{W}(t) = \mathbf{W}(t+dt) - \mathbf{W}(t)$. When $f(t, \mathbf{X}(t))$ denotes a continuous function which is one-time differentiable with respect to t and twice differentiable with respect to $\mathbf{X}(t)$, then the random process $f(t, \mathbf{X}(t))$ can be represented by using the Itô formula as shown in the following equation.

$$df(t, \mathbf{X}(t)) = \left[\frac{\partial f}{\partial t}(t, \mathbf{X}(t)) + \sum_{k=1}^i \frac{\partial}{\partial X_k} f(t, \mathbf{X}(t)) a_k(t) + \frac{1}{2} \sum_{m=1}^j \sum_{k,l=1}^i \frac{\partial^2}{\partial X_k \partial X_l} f(t, \mathbf{X}(t)) b_{km}(t) b_{lm}(t) \right] dt \quad (15)$$

$$+ \sum_{m=1}^j \sum_{k=1}^i \frac{\partial f}{\partial X_k}(t, \mathbf{X}(t)) b_{km}(t) dW_m(t)$$

Taking the average on both sides of Eq. (15) results in

$$\frac{d}{dt} \mathbb{E}[f(\mathbf{X})] = \sum_{k=1}^i \mathbb{E} \left[\frac{\partial f(\mathbf{X})}{\partial X_k} a_k(t) \right] + \frac{1}{2} \sum_{m=1}^j \sum_{k,l=1}^i \mathbb{E} \left[\frac{\partial^2 f(\mathbf{X})}{\partial X_k \partial X_l} b_{km}(t) b_{lm}(t) \right]. \quad (16)$$

Here, $\mathbb{E}[dW] = 0$ is used, and $f(\mathbf{X})$ is denoted as

$$f(\mathbf{X}) = \prod_{k=1}^i X_k^{C_k} = X_1^{C_1} X_2^{C_2} \cdots X_i^{C_i}. \quad (17)$$

Then, ordinary differential equations for the moments can be derived from Eq. (16).

Next, the moment equations are derived from the equations of motion of parametric rolling [24] as Eq.(18).

$$\ddot{\phi} + \beta_1 \dot{\phi} + \beta_3 \phi^3 + \omega_0^2 \sum_{n=1}^5 \gamma_{2n-1} \phi^{2n-1} + F(y_1) \phi = 0 \quad (18)$$

where

$$F(y_1) = \frac{\omega_0^2}{GM} \sum_{n=1}^{12} \rho_n y_1^n. \quad (19)$$

Here, ϕ , $\dot{\phi}$, $\ddot{\phi}$, and y_1 denote the roll angle, the roll velocity, the roll angular acceleration, and the effective wave elevation, respectively. Moreover, β_1 is the linear and β_3 is the cubic damping coefficient divided by I_{xx} , I_{xx} is the moment of inertia in roll (including the corresponding added moment of inertia), γ_i ($i = 1, 3, 5, 7, 9$) is the coefficient of the i -th component of the polynomial fitted GZ curve, and ρ_i ($i = 1, 2, \dots, 12$) is the coefficient of the i -th component of the polynomial, which fits the relationship between ΔGM and wave elevation at amidships in Fig. 4. Finally, ω_0 denotes the natural roll frequency.

In this study, the resulting system of equations is represented by means of the following 8th-order Itô SDE, which consists of a second-order SDE for the ship motion and a 6th-order SDE for the effective wave.

$$\begin{cases} dX_1 = X_2 dt \\ dX_2 = \{-G(X_1, X_2) - F(y_1)X_1\} dt \\ dy_1 = (y_2 - \alpha_1 y_1) dt \\ dy_2 = (y_3 - \alpha_2 y_1) dt \\ dy_3 = (y_4 - \alpha_3 y_1) dt + \sqrt{\pi} k dW(t), \\ dy_4 = (y_5 - \alpha_4 y_1) dt \\ dy_5 = (y_6 - \alpha_5 y_1) dt \\ dy_6 = -\alpha_6 y_1 dt \end{cases} \quad (20)$$

where

$$G(X_1, X_2) = \beta_1 X_2 + \beta_3 X_2^3 + \omega_0^2 \sum_{n=1}^5 \gamma_{2n-1} X_1^{2n-1}, \quad (21)$$

Here, X_1 and X_2 denote the roll angle and the roll velocity. The notation of variables of the linear filter is rewritten, as $y_1 = X_3, y_2 = X_4, y_3 = X_5, y_4 = X_6, y_5 = X_7, y_6 = X_8$. Summarizing Eq. (20) in a matrix form like Eq. (13), the components of drift and diffusion are as follows:

$$a_1 = X_2, a_2 = -G(X_1, X_2) - F(X_3)X_1, a_3 = X_4 - \alpha_1 X_3,$$

$$a_4 = X_5 - \alpha_2 X_3, a_5 = X_6 - \alpha_3 X_3, a_6 = X_7 - \alpha_4 X_3,$$

$$a_7 = X_8 - \alpha_5 X_3, a_8 = -\alpha_6 X_3,$$

$$b_{ij} = \begin{cases} \sqrt{\pi} k & (i = j = 5) \\ 0 & \text{otherwise} \end{cases}$$

By using $f(\mathbf{X}) = \prod_{k=1}^8 X_k^{C_k}$,

$$\frac{\partial f(\mathbf{X})}{\partial X_k} = \frac{C_k}{X_k} f(\mathbf{X}), \quad \frac{\partial^2 f(\mathbf{X})}{\partial X_k^2} = \frac{C_k(C_k - 1)}{X_k^2} f(\mathbf{X}). \quad (23)$$

Finally, the moment equation for the system in Eq. (20) is represented as:

$$\begin{aligned} \frac{d}{dt} \mathbb{E}[f(\mathbf{X})] &= \sum_{k=1}^8 \mathbb{E} \left[\frac{\partial f(\mathbf{X})}{\partial X_k} a_k(t) \right] \\ &+ \frac{1}{2} \sum_{m=1}^8 \sum_{k,l=1}^8 \mathbb{E} \left[\frac{\partial^2 f(\mathbf{X})}{\partial X_k \partial X_l} b_{km}(t) b_{lm}(t) \right] \\ &= C_1 \mathbb{E} \left[X_1^{C_1-1} X_2^{C_2+1} X_3^{C_3} X_4^{C_4} X_5^{C_5} X_6^{C_6} X_7^{C_7} X_8^{C_8} \right] \\ &- C_2 \mathbb{E} \left[G(X_1, X_2) X_1^{C_1} X_2^{C_2-1} X_3^{C_3} X_4^{C_4} X_5^{C_5} X_6^{C_6} X_7^{C_7} X_8^{C_8} \right] \\ &- C_2 \mathbb{E} \left[F(X_3) X_1^{C_1+1} X_2^{C_2-1} X_3^{C_3} X_4^{C_4} X_5^{C_5} X_6^{C_6} X_7^{C_7} X_8^{C_8} \right] \\ &+ C_3 \mathbb{E} \left[(X_4 - \alpha_1 X_3) X_1^{C_1} X_2^{C_2} X_3^{C_3-1} X_4^{C_4} X_5^{C_5} X_6^{C_6} X_7^{C_7} X_8^{C_8} \right] \\ &+ C_4 \mathbb{E} \left[(X_5 - \alpha_2 X_3) X_1^{C_1} X_2^{C_2} X_3^{C_3} X_4^{C_4-1} X_5^{C_5} X_6^{C_6} X_7^{C_7} X_8^{C_8} \right] \\ &+ C_5 \mathbb{E} \left[(X_6 - \alpha_3 X_3) X_1^{C_1} X_2^{C_2} X_3^{C_3} X_4^{C_4} X_5^{C_5-1} X_6^{C_6} X_7^{C_7} X_8^{C_8} \right] \\ &+ C_6 \mathbb{E} \left[(X_7 - \alpha_4 X_3) X_1^{C_1} X_2^{C_2} X_3^{C_3} X_4^{C_4} X_5^{C_5} X_6^{C_6-1} X_7^{C_7} X_8^{C_8} \right] \\ &+ C_7 \mathbb{E} \left[(X_8 - \alpha_5 X_3) X_1^{C_1} X_2^{C_2} X_3^{C_3} X_4^{C_4} X_5^{C_5} X_6^{C_6} X_7^{C_7-1} X_8^{C_8} \right] \\ &- \alpha_6 C_8 \mathbb{E} \left[X_1^{C_1} X_2^{C_2} X_3^{C_3+1} X_4^{C_4} X_5^{C_5} X_6^{C_6} X_7^{C_7} X_8^{C_8-1} \right] \\ &+ \frac{\pi k^2}{2} C_5(C_5 - 1) \mathbb{E} \left[X_1^{C_1} X_2^{C_2} X_3^{C_3} X_4^{C_4} X_5^{C_5-2} X_6^{C_6} X_7^{C_7} X_8^{C_8} \right] \end{aligned} \quad (24)$$

From Eq. (24), the eight first-order and thirty-six second-order moment equations are obtained as shown in Appendix 2.

The first-order and second-order moment equations can be derived from the SDE with the nonlinear components and the non-Gaussian excitation process. Furthermore, higher-order moment equations can be generated from Eq.(24) such as one hundred twenty third-order and three hundred thirty fourth-order moment equations. In general, a nonlinear system generates an infinite hierarchy of moment equations. The system in this study is the nonlinear system given in Eq.(20). In order to form a closed set of moment equations, higher-order moments need to be truncated. To solve

this problem, higher-order moments need to be expressed by lower-order moments. Therefore, the cumulant neglect closure method[42][43][44] is used in this study. In particular, the second-order cumulant neglect method is used, which ignores cumulants of higher than the third-order. In other words, the third and higher-order cumulants are set to zero. This closure method is the same as the Gaussian closure method, because the third and higher-order cumulants of a Gaussian distribution are zero. In this study, the first and second-order moment equations include the third and higher-order moments as shown in Eqs.(33) and (34) of Appendix2. Hence, the third and higher-order moments need to be represented using first and second-order moments. The relationship between the lower and the higher-order moments can be obtained using the cumulant neglect closure method. Comparing the coefficients of series expansions of a moment generating function and a cumulant generating function, the relations between moments and cumulants can be obtained. The detailed derivation procedure of their relations is shown in Appendix 3. Using these relations, the higher-order moments can be represented by the lower-order moments. As a result, the moment equations can be written in a closed form, and the moment values can be obtained from them.

4 Calculation results

In this study, the numerical simulations by means of the superposition principle and by solving the SDE are analysed. And the moment equations are solved. Furthermore, two types of the arbitrary PDF and the objective function are set.

4.1 Subject ship

In order to validate the moment equation method, the results are compared with numerical simulations. In this study, for a subject ship, the calculation results are compared for the Froude number $F_n = 0.00$ and 0.04 in head seas. Please note that in the considered case the choice of Froude number $F_n=0.00$ leads to most severe parametric rolling conditions. Here, the C11 class post-Panamax containership [45] is used as the subject ship. The body plan and principal particulars of this ship is shown in Fig. 8 and Table 3, respectively. Fig. 9 shows the GZ curve for the C11 containership, resulting from hydrostatic calculations in calm water. This restoring arm is calculated based on the Froude-Krylov hypothesis [40]. In this study, the actual GZ is approximated by a 9th order polynomial in order to provide a reasonable GZ curve. As shown in Fig. 9, the C11 containership has a GZ curve which is linear up to a roll angle of around 40 degrees. The calculation condition in this study is that the wave mean period T_{01} is 9.99[s] and the significant wave height $H_{1/3}$ is

5.0[m]. In order to validate the use of moment equations, a sea condition is chosen such that the probability of capsizing is practically zero. Also, the roll damping coefficients are estimated by Ikeda's simplified method [46]. As a result, the damping coefficients are obtained as $\beta_1 = 3.64 \times 10^{-3}$, $\beta_3 = 4.25$ with $F_n = 0.00$ and $\beta_1 = 2.14 \times 10^{-3}$, $\beta_3 = 4.25$ with $F_n = 0.04$.

Table 3: Principal Particulars of the subject ship at full scale

Items	C11
Length: L_{pp}	262.0 [m]
Breadth: B	40.0 [m]
Depth: D	24.45 [m]
Draught: d	11.5 [m]
Block coefficient: C_b	0.562
Metacentric height: GM	1.965 [m]
Natural roll period: T_ϕ	25.1 [s]
Bilge keel length ratio: L_{BK}/L_{pp}	0.292
Bilge keel breadth ratio: B_{BK}/B	0.0100

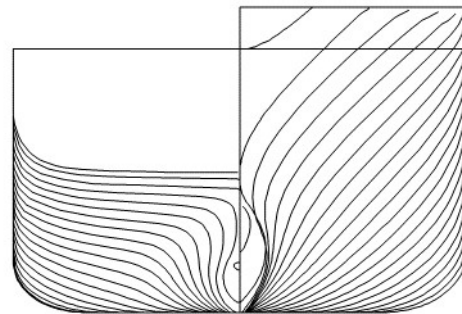


Fig. 8: Body Plan (C11)

4.2 Calculation of moment equations

In order to compare the moment values obtained by solving the moment equations, the numerical simulation of the superposition principle and the SDE are explained first. The numerical simulation using the superposition principle is computed by means of the 4th order Runge–Kutta method, while the numerical simulation of the SDE Eq. (20) is computed using the Euler-Maruyama method[37]. The time step is set such that the former is 0.02[s] and the latter is 0.001[s]. Both initial conditions are set to a roll angle of 5[deg.] and a roll velocity of 0[deg./s]. The number of realizations of the

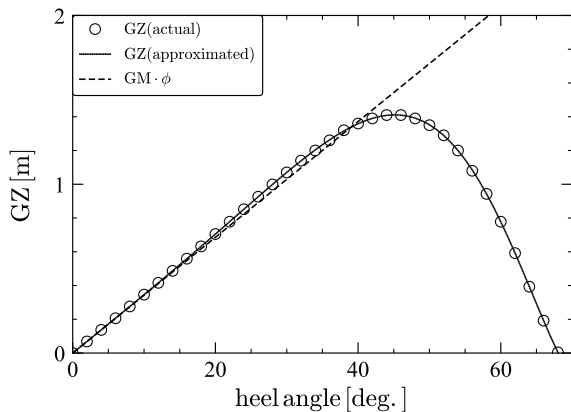


Fig. 9: GZ curve in still water (C11)

numerical simulation is 100, and each simulation time is 1 hour.

Next, the ordinary differential equations for the moment equations (Eq. (33) and (34)) are explained. These equations are computed using the 4th order Runge–Kutta method as an initial value problem. The initial condition for all moments is set to a value of 0.01. Here, the time step is set to 0.01[s]. In this study, it should be noted that the moment equations are calculated in an unsteady state. The calculation of moment equations in steady-state needs to solve simultaneous nonlinear equations. Then the solutions can be obtained by using the Newton-Raphson method and Jacobian matrix. The convergence and the corresponding matrix calculation are complex. On the other hand, the region of steady state can be determined easily from the computation of the corresponding ordinary differential equation. Furthermore, we consider that it is an appropriate method from the perspective of unaffected on the number of moment equations.

Table 4: Moment values obtained by solving SDE (Eq.(20)) and numerical simulation using the superposition principle, with $F_n = 0.00$.

	Superposition	SDE
$\mathbb{E}[X_1]$	-2.00×10^{-5}	1.10×10^{-5}
$\mathbb{E}[X_1^2]$	4.59×10^{-2}	4.61×10^{-2}
$\mathbb{E}[X_2]$	-9.56×10^{-6}	-6.94×10^{-6}
$\mathbb{E}[X_2^2]$	2.94×10^{-3}	2.95×10^{-3}
$\mathbb{E}[X_3]$	-1.54×10^{-5}	7.10×10^{-6}
$\mathbb{E}[X_3^2]$	0.792	0.796

An example of computation results is shown in Fig. 10. This figure shows the displacement of second-moment of

Table 5: Moment values obtained by solving the moment equations (Eq.(33) and (34)) and by solving SDE (Eq.(20)), with $F_n = 0.00$.

	SDE	Moment eq. (2nd)
$\mathbb{E}[X_1]$	1.10×10^{-5}	-2.01×10^{-4}
$\mathbb{E}[X_1^2]$	4.61×10^{-2}	3.50×10^{-2}
$\mathbb{E}[X_2]$	-6.94×10^{-6}	-2.27×10^{-4}
$\mathbb{E}[X_2^2]$	2.95×10^{-3}	2.25×10^{-3}
$\mathbb{E}[X_3]$	7.10×10^{-6}	0.00
$\mathbb{E}[X_3^2]$	0.796	0.794

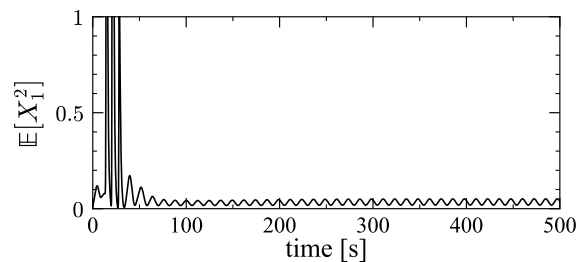


Fig. 10: Displacement of $\mathbb{E}[X_1^2]$ obtained by computing the ordinary differential equations for moments (Eq. (33) and (34)) with $F_n = 0.00$.

X_1 . As time increases, this displacement converges to the steady-state. Fig. 11 shows the displacement of first and second-order moments of X_1, X_2 , and X_3 in steady-state. The moment values of the right column in Table 5 are determined by taking the mean of the steady state displacement of the respective moments. In Fig. 11, the red dashed line denotes these moment values. Also, the blue dashed line denotes the moment values obtained by computing the SDE of Eq. (20) numerically. As shown in Fig. 11, the solution in steady-state is oscillatory. When the cumulant neglect order is of third order, it is noteworthy that this oscillation vanishes and the moment values become close to the moment values derived from numerical computations of the SDE, as shown in Appendix 4. Moreover, it is observed in Fig. 3 that the Gaussian distribution using mean and variance obtained from the moment equations agrees with the PDF obtained by solving the SDE of linear filter numerically in all range. The agreement at the peak from the left panel of Fig. 3 and the tail from the right panel of Fig. 3 can be observed, respectively.

It can be obtained in the same way. Table 6 shows the respective calculation results obtained by using the superposition principle, solving the SDE of Eq. (20), and solving the moment equations of Eqs.(33) and (34).

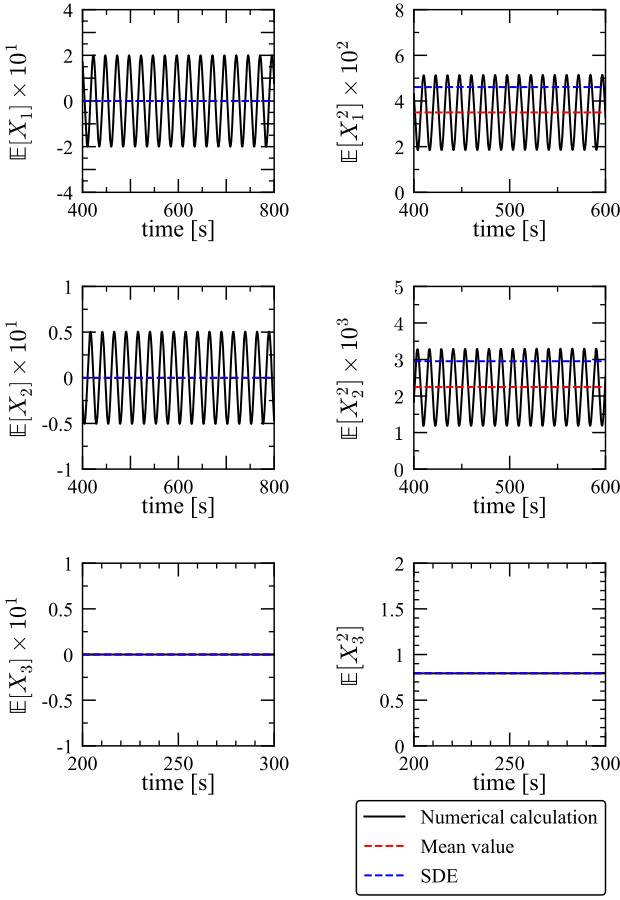


Fig. 11: First and second order moment of X_1, X_2, X_3 obtained by computing the ordinary differential equations for moments (Eq. (33) and (34)), and moment values from SDE (Table 4), with $F_n = 0.00$.

Table 6: Moment values obtained by solving the moment equations (Eqs.(33) and (34)) and by solving SDE (Eq.(20)), with $F_n = 0.04$.

	Superposition	SDE	Moment eq. (2nd)
$\mathbb{E}[X_1]$	-1.56×10^{-5}	-1.25×10^{-5}	-7.41×10^{-4}
$\mathbb{E}[X_1^2]$	3.21×10^{-2}	3.28×10^{-2}	2.51×10^{-2}
$\mathbb{E}[X_2]$	7.29×10^{-6}	4.43×10^{-6}	4.13×10^{-5}
$\mathbb{E}[X_2^2]$	2.16×10^{-3}	2.21×10^{-3}	1.67×10^{-3}
$\mathbb{E}[X_3]$	9.50×10^{-6}	1.23×10^{-5}	0.00
$\mathbb{E}[X_3^2]$	0.792	0.807	0.804

4.3 Procedure for determining the PDF, and results

Based on the moment values in Table 5 by computing the moment equations, the PDF of roll angle is determined. In this study, the following non-Gaussian PDF shape types are

set. The shape of type1 is proposed by Maki [31] and type2 is inspired from the Laplace distribution. The Laplace distribution itself is similar in the function shape, however, cannot have a good fitting result in all ranges. Therefore, new terms are added in the exponent component like Eq.(26) in this study.

type1 :

$$\mathcal{P}_1(X_1) = C \exp \left\{ - (d_1 X_1 + d_2 X_1^2 + d_3 X_1^3 + d_4 X_1^4) \right\} \quad (25)$$

type2 :

$$\mathcal{P}_2(X_1) = C \exp \left\{ - (d_1 |X_1| + d_2 |X_1|^2 + d_3 |X_1|^3 + d_4 |X_1|^4) \right\} \quad (26)$$

Here, C is a normalization constant. In order to determine the coefficients of Eqs. (25) and (26), the following expression is suggested.

$$J_n = \int_{-\infty}^{+\infty} X_1^n \mathcal{P}(X) dX - \mathbb{E}[X_1^n] \quad (27)$$

The moment values, which are obtained by solving the moment equations in Eq. (33) and (34), are the first- and the second-order moments, only. Hence, higher-order moment values need to be obtained by using the cumulant neglect closure method as shown in Appendix 3. Furthermore, the following objective function $J(d_1, d_2, d_3, d_4)$ is set.

$$J(d_1, d_2, d_3, d_4) = \sum_{i=1}^6 l_i |J_i| \quad (28)$$

Here, l_i are weights and $l_i = 1 (i = 1, 2, \dots, 6)$. In this case, up to sixth-order moments are used for the determination of the coefficients.

As shown in Fig. 12, it can be observed that the time series of roll angle, which is obtained by solving the SDE, shows a typical parametric rolling behaviour. As shown in Fig. 13, it can be observed that the PDF of roll angle obtained by solving the SDE agrees with the PDF obtained by using the superposition principle. The agreement at the peak from the left panel of Fig. 13 and the tail from the right panel of Fig. 13 can be observed, respectively. However, these PDFs do not agree with a Gaussian distribution.

Fig. 14 shows the optimized result of PDFs of type 1 and type 2. Here, the moment values obtained by solving the moment equations are used. Applying the PDF of type 1, the obtained PDF has a similar function shape as a Gaussian distribution. This is because the second-order moment has a larger value than the other moments. We should focus on the point that the PDF of roll angle and the Laplace distribution resemble the function form. Therefore, in this study, Eq. (26)

is defined. As a result of using type 2, the optimized function has an improved agreement in shape with the numerical simulation result.

As we have seen, the moment values have a difference between the numerical result and the moment equation result. Thus, the moment values from the SDE results in Table 4 are used. In Fig. 15, the optimized PDF of type 2 (the red dashed line) matches with the SDE result (the black solid line). Here, the agreement at the peak from the left panel of Fig. 15 and the tail from the right panel of Fig. 15 can also be observed, respectively. Therefore, it is clear that the optimized PDF, which agrees with the numerical simulation result, can be obtained by using accurate moment values and the PDF of type 2. In addition, for the case of $F_n = 0.04$ the results from Fig. 16 also show that the optimized PDF of type 2 matches with the SDE result. Therefore, it is confirmed that the PDF for a case with a forward velocity can be obtained using our proposed method.

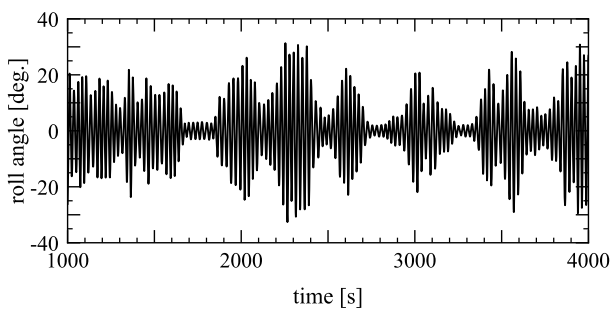


Fig. 12: Time series of roll angle obtained by solving SDE (Eq. (20)), with $F_n = 0.00$.

5 Concluding remarks

It has been observed that the time series of the effective wave can be modeled sufficiently by using a linear filter. Furthermore, it turns out that the time series of GM variation can be modeled sufficiently by using the linear filter and the relationship between ΔGM and wave elevation.

We have summarized a procedure in which the moment equations are obtained from a higher-order stochastic differential equation. Furthermore, we have suggested a simple way to calculate the steady state results for the moments. The appropriate moment values can be obtained easily for a higher-order SDE. Most important of all is the non-Gaussian PDF can be obtained by using the appropriate values for our proposed PDF and objective function.

In this study, the linear filter was used for the effective wave. We examine this filter whether it can be used for

the methodology of GM variation and GZ variation. Further studies are needed in order to determine a set of probability density functions which have the shape of the objective probability densities. Moreover, our proposed method can be applied to a multi-degree of freedom model if this system can be represented by a polynomial. Therefore, we will investigate our proposed method for the case of a multi-degree of freedom model in future research. Although, the probability of the one degree of freedom model is evaluated on the safer side than that of the multi degree of freedom model. Therefore, to estimate the probability theoretically and quickly is useful for practical purposes.

Acknowledgements This work was supported by a Grant-in-Aid for Scientific Research from the Japan Society for Promotion of Science (JSPS KAKENHI Grant Number 19H02360) and by Support for Pioneering Research Initiated by the Next Generation from Japan Science and Technology Agency (JST SPRING, Grant Number JPMJSP2138), as well as the collaborative research program / financial support from the Japan Society of Naval Architects and Ocean Engineers. This study was supported by the Fundamental Research Developing Association for Shipbuilding and Offshore (REDAS), managed by the Shipbuilders' Association of Japan from April 2020 to March 2023.

References

1. L. Dostal, E. Kreuzer, Probabilistic approach to large amplitude ship rolling in random seas, *Proceedings of the Institution of Mechanical Engineers, Part C: Journal of Mechanical Engineering Science* **225**(10), 2464 (2011)
2. P.T.D. Spanos, ARMA algorithms for ocean wave modeling, *Journal of Energy Resources Technology* **105**(3), 300 (1983)
3. P.T.D. Spanos, Filter approaches to wave kinematics approximation, *Applied Ocean Research* **8**(1), 2 (1986)
4. J.O. Flower, N. Vije, A note on ratio-of-polynomials curve-fitting of seawave spectra, *International Shipbuilding Progress* **30**(341), 10 (1983)
5. J.O. Flower, N. Vije, Further considerations of the ratio-of-polynomials form-fit of seawave spectra, *International Shipbuilding Progress* **32**(365), 2 (1985)
6. S.K. Thampi, J.M. Niedzwecki, Filter approach to ocean structure response prediction, *Applied Ocean Research* **14**(4), 259 (1992)
7. A.B. Degtyarev, A.M. Reed, Modeling of incident waves near the ship's hull (application of autoregressive approach in problems of simulation of rough seas), *Proceedings of the 12th International Ship Stability Workshop, Washington D.C., USA* pp. 175–187 (2011)
8. A.B. Degtyarev, I. Gankevich, Evaluation of hydrodynamic pressures for autoregressive model of irregular waves, *Proceedings of the 11th International Conference on the Stability of Ships and Ocean Vehicles, Athens, Greece* pp. 841–851 (2012)
9. C. Nichita, D. Luca, B. Dakyo, E. Ceanga, Large band simulation of the wind speed for real time wind turbine simulators, *IEEE Transactions on Energy Conversion* **17**(4), 523 (2002)
10. L. Dostal, M. Hollm, E. Kreuzer, Study on the behavior of weakly nonlinear water waves in the presence of random wind forcing, *Nonlinear Dynamics* **99**, 2319 (2020)
11. A. Maki, Y. Maruyama, L. Dostal, M. Sakai, R. Sawada, K. Sasa, N. Umeda, Practical methodology of wind process generation for examining autonomous operating systems of ships, *Journal of Marine Science and Technology* p. on line first (2021)

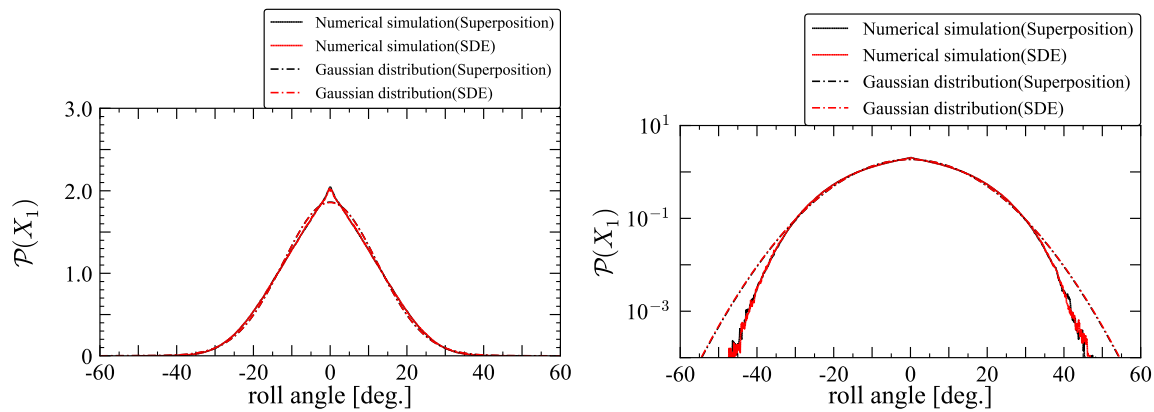


Fig. 13: Comparison of PDF of X_1 among result obtained by solving SDE (Eq. (20)) : Numerical simulation (SDE), numerical simulation result by a principle of superposition : Numerical simulation (Superposition), and Gaussian distributions by using moment values (Table 4), with $F_n = 0.00$.

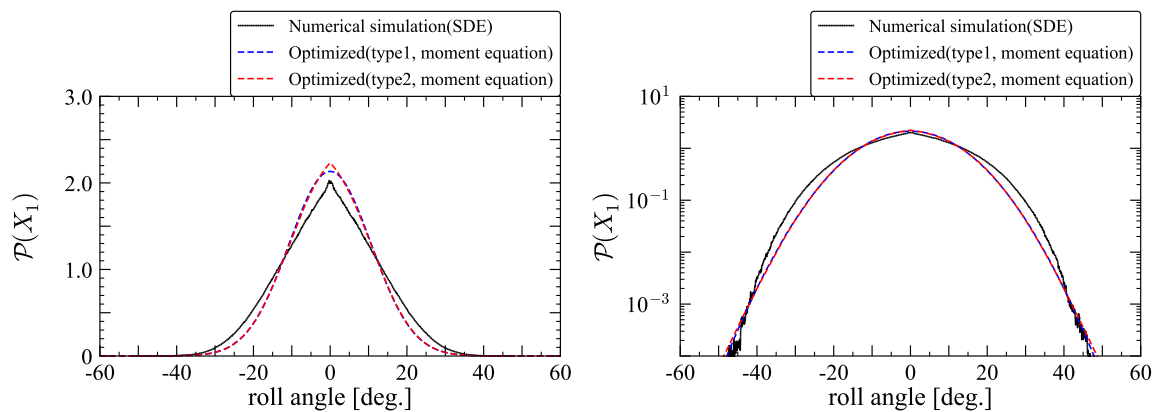


Fig. 14: Comparison of PDF of X_1 among result obtained by solving SDE (Eq. (20)) : Numerical simulation (SDE), optimized result by using Eq. (25) and moment values (Table 5) obtained by solving moment equations (Eq. (33) and (34)) : optimized (type 1, moment equation), and optimized result by using Eq. (26) and moment values (Table 5) obtained by solving moment equations (Eq. (33) and (34)) : optimized (type 2, moment equation), with $F_n = 0.00$.

12. K. Watanabe, On the dynamical properties of the transverse instability of a ship due to pitching, *Journal of the Society of Naval Architects of Japan* (in Japanese) pp. 51–70 (1934)
13. J.E. Kerwin, Notes on rolling in longitudinal waves, *International Shipbuilding Progress* **2**(16), 597 (1955)
14. H. Hashimoto, N. Umeda, Y. Ogawa, H. Taguchi, T. Iseki, G. Bulian, N. Toki, S. Ishida, A. Matsuda, Prediction methods for parametric rolling with forward velocity and their validation-final report of the scape committee (part 2), *Proc 6th Osaka Colloquium on Seakeeping and Stability of Ships*, Osaka, Japan pp. 265–275 (2008)
15. G. Bulian, A. Francescutto, N. Umeda, H. Hashimoto, Qualitative and quantitative characteristics of parametric ship rolling in random waves in the light of physical model experiments, *Ocean Engineering* **35**(17), 1661 (2008)
16. N. Umeda, M. Sakai, N. Fujita, A. Morimoto, D. Terada, A. Matsuda, Numerical prediction of parametric roll in oblique waves, *Ocean Engineering* **120**, 212 (2016)
17. IMO, Interim guidelines on the second generation intact stability criteria, *MSC.1/Circ 1627* pp. 1–60 (2020)
18. IMO, Simplified operational guidance from level 2 vulnerability assessment for parametric roll, *SDC 8/WP.4/Add.5* pp. 37–40 (2022)
19. T.K. Caughey, Derivation and application of the fokker-planck equation to discrete nonlinear dynamic systems subjected to white random excitation., *Journal of the Acoustical Society of America* **35**(11), 1683 (1963)
20. T.K. Caughey, Equivalent linearization techniques., *Journal of the Acoustical Society of America* **35**(11), 1706 (1963)
21. L. Socha, *Linearization Methods for Stochastic Dynamic Systems*. Lecture notes in physics (Springer-Verlag Berlin Heidelberg, 2008)
22. L. Dostal, E. Kreuzer, N. Sri Namachchivaya, Non-standard stochastic averaging of large-amplitude ship rolling in random seas., *Proceedings: Mathematical, Physical and Engineering Sciences* **468**(2148), 4146 (2012)
23. J.B. Roberts, Effect of parametric excitation on ship rolling motion in random waves., *Journal of Ship Research* **26**(4), 246 (1982)
24. Y. Maruyama, A. Maki, L. Dostal, N. Umeda, Improved stochastic averaging method using hamiltonian for parametric rolling in irregular longitudinal waves., *Journal of Marine Science and Technology* (2021)

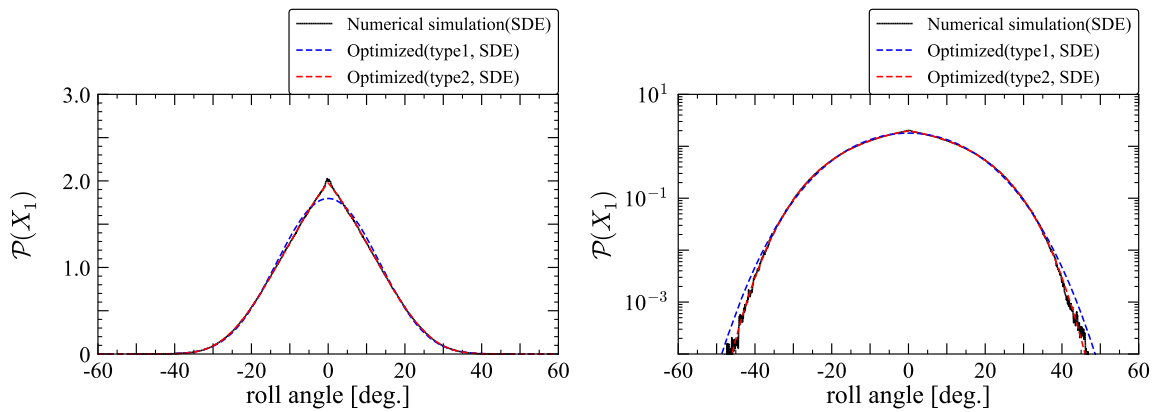


Fig. 15: Comparison of PDF of X_1 among result obtained by solving SDE (Eq. (20)) : Numerical simulation (SDE), optimized result by using Eq.(25) and moment values (Table 5) obtained by calculating SDE (Eq. (20)) : optimized (type 1, SDE), and optimized result by using Eq.(26) and moment values (Table 5) obtained by calculating SDE (Eq. (20)) : optimized (type 2, SDE), with $F_n = 0.00$.

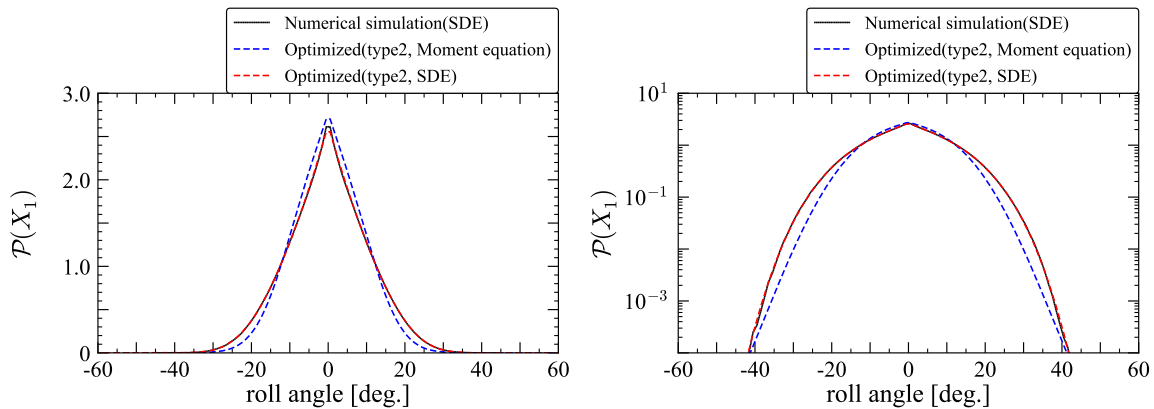


Fig. 16: Comparison of PDF of X_1 among result obtained by solving SDE (Eq. (20)) : Numerical simulation (SDE), optimized result by using Eq.(26) and moment values (Table 6) obtained by solving moment equations (Eq. (33) and (34)) : optimized (type 2, moment equation), and optimized result by using Eq.(26) and moment values (Table 6) obtained by calculating SDE (Eq. (20)) : optimized (type 2, SDE), with $F_n = 0.04$.

25. D.C.C. Bover, Moment equation methods for nonlinear stochastic systems, *Journal of Mathematical Analysis and Applications* **65**(2), 306 (1978)
26. W.F. Wu, Comparison of gaussian closure technique and equivalent linearization method., *Probabilistic Engineering Mechanics* **2**, 2 (1987)
27. V.A. Nekrasov, Stochastic stability theory of ship motions, *Proceedings of the 5th International Conference on the Stability of Ships and Ocean Vehicles*, Melbourne, Florida, USA **5**, 841 (1994)
28. K. Yokoyama, K. Kimura, Non-gaussian response characteristics of an asymmetric nonlinear system subjected to nonwhite excitation (relationship between non-gaussianity and resonance), *Transactions of the Japan Society of Mechanical Engineers Series C* **79**(799), 573 (2013), (in Japanese)
29. V. Belenky, K.M. Weems, On the distribution of parametric roll., *Proceedings of the 12th International Ship Stability Workshop*, Washington D.C., USA pp. 205–212 (2011)
30. M.A. Mohamad, T.P. Sapsis, Probabilistic response and rare events in mathieu's equation under correlated parametric excitation, *Ocean Engineering* **120**, 289 (2016)
31. A. Maki, Estimation method of the capsizing probability in irregular beam seas using non-gaussian probability density function, *Journal of Marine Science and Technology* **22**, 351 (2017)
32. A. Francescutto, S. Naito, Large amplitude rolling in a realistic sea., *Proceedings of the 8th International Conference on Stability of Ships and Ocean Vehicles*, Madrid, Spain pp. 495–505 (2003)
33. Z. Su, J.M. Falzarano, Gaussian and non-gaussian cumulant neglect application to large amplitude rolling in random waves., *International shipbuilding progress* **58**(2-3), 97 (2011)
34. W. Chai, A. Naess, B.J. Leira, G. Bulian, Efficient monte carlo simulation and grim effective wave model for predicting the extreme response of a vessel rolling in random head seas., *Ocean Engineering* **123**, 191 (2016)
35. O. Grim, Beitrag zu dem problem der sicherheit des schiffes in seegang., *Schiff und Hafen* **6** pp. 490–497 (1961)
36. N. Umeda, M. Ariji, Y. Yamakoshi, Assessment for probability of ship capsizing due to pure loss of stability in quartering seas (2nd report), *Journal of the Kansai Society of Naval Architects*, Japan **216**, 129 (1991)

37. G. Maruyama, Continuous Markov processes and stochastic equations, *Rendiconti del Circolo Matematico di Palermo* **4**(1), 48 (1955)
38. M. Shuku, H. Shimada, H. Fujii, S. Toyoda, K. Ikegami, H. Ando, The motions of moored floating storage barge in shallow water (non-linear mathematical model and numerical simulation) (in Japanese), *Journal of the Society of Naval Architects of Japan* **1979**(146), 245 (1979)
39. N. Umeda, Y. Yamakoshi, Probability of ship capsizing due to pure loss of stability in quartering seas., *Naval architecture and ocean engineering* **30**, 73 (1992)
40. M. Hamamoto, Y. Kim, K. Uwatoko, Study on ship motions and capsizing in following seas (final report), *Journal of the Society of Naval Architects of Japan* **1991**(170), 173 (1991)
41. K. Sobczyk, *Stochastic Differential Equations With Applications to Physics and Engineering*. Mathematics and Its Applications. (Springer Netherlands, 1991)
42. J.Q. Sun, C.S. Hsu, Cumulant-neglect closure method for nonlinear systems under random excitations., *Journal of applied mechanics* **54**(3), 649 (1987)
43. J.Q. Sun, C.S. Hsu, Cumulant-neglect closure method for asymmetric non-linear systems driven by gaussian white noise., *Journal of sound and vibration* **135**(2), 338 (1989)
44. S.F. Wojtkiewicz, B.F. Spencer, L.A. Bergman, On the cumulant-neglect closure method in stochastic dynamics., *International Journal of Non-Linear Mechanics* **31**(5), 657 (1996)
45. H. Hashimoto, N. Umeda, A study on quantitative prediction of parametric roll in regular waves., *Proceedings of the 11th International Ship Stability Workshop, Wageningen, The Netherlands* pp. 295–301 (2010)
46. Y. Kawahara, K. Maekawa, Y. Ikeda, A simple prediction formula of roll damping of conventional cargo ships on the basis of ikeda's method and its limitation., *Journal of Shipping and Ocean Engineering* **2**(4), 201 (2012)

Appendix 1

In this study, we use the ARMA filter. Here, the 2nd, 4th, and 6th-order ARMA filter are compared. First, the ordinary differential equations of the 2nd and 4th-order ARMA filter are expressed as follows:

$$\begin{cases} \frac{dx_1}{dt} = x_2 - \alpha_1 x_1 + \sqrt{\pi}k \frac{dW(t)}{dt} \\ \frac{dx_2}{dt} = -\alpha_2 x_1 \end{cases} \quad (29)$$

$$\begin{cases} \frac{dx_1}{dt} = x_2 - \alpha_1 x_1 \\ \frac{dx_2}{dt} = x_3 - \alpha_2 x_1 + \sqrt{\pi}k \frac{dW(t)}{dt} \\ \frac{dx_3}{dt} = x_4 - \alpha_3 x_1 \\ \frac{dx_4}{dt} = -\alpha_4 x_1 \end{cases} \quad (30)$$

Here, W denotes the standard Wiener process, and the notation for differentiation is represented by Lagrange's notation. As discussed later, the coefficients $\alpha_i (i = 1, \dots, 4)$ and k are determined such that they agree with the effective wave spectrum. From Eqs.(29) and (30), the spectra of the 2nd and 4th-order ARMA process can be obtained as:

$$S_2(\omega) = \frac{k^2 \omega^2}{(\omega^2 - \alpha_2)^2 + \alpha_1^2 \omega^2} \quad (31)$$

$$S_4(\omega) = \frac{k^2 \omega^4}{(\omega^4 - \alpha_2 \omega^2 + \alpha_4)^2 + (\alpha_1 \omega^3 - \alpha_3 \omega)^2} \quad (32)$$

Next, the coefficients α_i and k of Eqs.(10), (31), and (32) are determined by fitting the effective wave spectrum. Here, the stability criterion of their corresponding system explained in section2 is used. In Fig.17, the effective wave spectrum, 2nd, 4th, and 6th-order ARMA spectra are plotted. From this figure, we can see that the 6th-order ARMA filter is better than the 2nd and 4th-order ARMA filters. Therefore, the 6th-order ARMA filter is used in this study.

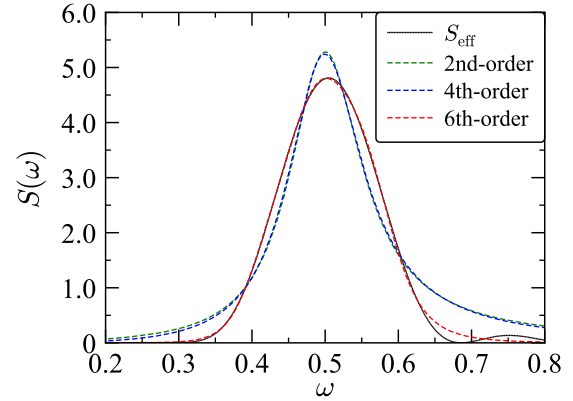


Fig. 17: Comparison among effective wave spectrum S_{eff} , 2nd-order ARMA spectrum S_2 , 4th-order ARMA spectrum S_4 , and 6th-order ARMA spectrum S_6 . Here, the sea condition is $T_{01} = 9.99[s]$ and $H_{1/3} = 5.0[m]$

Appendix 2

From Eq. (24), the following eight first-order moment equations are obtained:

$$\begin{aligned} \frac{d}{dt} \mathbb{E}[X_1] &= \mathbb{E}[X_2] \\ \frac{d}{dt} \mathbb{E}[X_2] &= -\mathbb{E}[G(X_1, X_2)] - \mathbb{E}[F(X_3)X_1] \\ \frac{d}{dt} \mathbb{E}[X_i] &= \mathbb{E}[X_{i+1}] - \alpha_{i-2} \mathbb{E}[X_3] \quad (i = 3 \dots 7) \\ \frac{d}{dt} \mathbb{E}[X_8] &= -\alpha_6 \mathbb{E}[X_3] \end{aligned} \quad (33)$$

Moreover, thirty-six second-order moment equations are obtained as:

$$\begin{aligned} \frac{d}{dt} \mathbb{E}[X_1^2] &= 2\mathbb{E}[X_1 X_2] \\ \frac{d}{dt} \mathbb{E}[X_1 X_2] &= \mathbb{E}[X_2^2] - \mathbb{E}[G(X_1, X_2)X_1] - \mathbb{E}[F(X_3)X_1^2] \\ \frac{d}{dt} \mathbb{E}[X_1 X_i] &= \mathbb{E}[X_2 X_i] + \mathbb{E}[X_1 X_{i+1}] \\ &\quad - \alpha_{i-2} \mathbb{E}[X_1 X_3] \quad (i = 3 \dots 7) \\ \frac{d}{dt} \mathbb{E}[X_1 X_8] &= \mathbb{E}[X_2 X_8] - \alpha_6 \mathbb{E}[X_1 X_3] \\ \frac{d}{dt} \mathbb{E}[X_2^2] &= -2\mathbb{E}[G(X_1, X_2)X_2] - 2\mathbb{E}[F(X_3)X_1 X_2] \end{aligned}$$

$$\begin{aligned} \frac{d}{dt} \mathbb{E}[X_2 X_i] &= -\mathbb{E}[G(X_1, X_2) X_i] - \mathbb{E}[F(X_3) X_1 X_i] \\ &\quad + \mathbb{E}[X_2 X_{i+1}] - \alpha_{i-2} \mathbb{E}[X_2 X_3] \quad (i = 3 \cdots 7) \end{aligned}$$

$$\begin{aligned} \frac{d}{dt} \mathbb{E}[X_2 X_8] &= -\mathbb{E}[G(X_1, X_2) X_8] - \mathbb{E}[F(X_3) X_1 X_8] \\ &\quad - \alpha_6 \mathbb{E}[X_2 X_3] \end{aligned}$$

$$\frac{d}{dt} \mathbb{E}[X_3^2] = 2\mathbb{E}[X_3 X_4] - 2\alpha_1 \mathbb{E}[X_3^2]$$

$$\begin{aligned} \frac{d}{dt} \mathbb{E}[X_3 X_i] &= \mathbb{E}[X_4 X_i] - \alpha_1 \mathbb{E}[X_3 X_i] \\ &\quad + \mathbb{E}[X_3 X_{i+1}] - \alpha_{i-2} \mathbb{E}[X_3^2] \quad (i = 4 \cdots 7) \end{aligned}$$

$$\frac{d}{dt} \mathbb{E}[X_3 X_8] = \mathbb{E}[X_4 X_8] - \alpha_1 \mathbb{E}[X_3 X_8] - \alpha_6 \mathbb{E}[X_3^2]$$

$$\frac{d}{dt} \mathbb{E}[X_4^2] = 2\mathbb{E}[X_4 X_5] - 2\alpha_2 \mathbb{E}[X_3 X_4]$$

$$\begin{aligned} \frac{d}{dt} \mathbb{E}[X_4 X_i] &= \mathbb{E}[X_5 X_i] - \alpha_2 \mathbb{E}[X_3 X_i] \\ &\quad + \mathbb{E}[X_4 X_{i+1}] - \alpha_{i-2} \mathbb{E}[X_3 X_4] \quad (i = 5 \cdots 7) \end{aligned}$$

$$\frac{d}{dt} \mathbb{E}[X_4 X_8] = \mathbb{E}[X_5 X_8] - \alpha_2 \mathbb{E}[X_3 X_8] - \alpha_6 \mathbb{E}[X_3 X_4]$$

$$\frac{d}{dt} \mathbb{E}[X_5^2] = 2\mathbb{E}[X_5 X_6] - 2\alpha_3 \mathbb{E}[X_3 X_5] + \pi k^2$$

$$\begin{aligned} \frac{d}{dt} \mathbb{E}[X_5 X_i] &= \mathbb{E}[X_6 X_i] - \alpha_3 \mathbb{E}[X_3 X_i] \\ &\quad + \mathbb{E}[X_5 X_{i+1}] - \alpha_{i-2} \mathbb{E}[X_3 X_5] \quad (i = 6, 7) \end{aligned}$$

$$\frac{d}{dt} \mathbb{E}[X_5 X_8] = \mathbb{E}[X_6 X_8] - \alpha_3 \mathbb{E}[X_3 X_8] - \alpha_6 \mathbb{E}[X_3 X_5]$$

$$\frac{d}{dt} \mathbb{E}[X_6^2] = 2\mathbb{E}[X_6 X_7] - 2\alpha_4 \mathbb{E}[X_3 X_6]$$

$$\begin{aligned} \frac{d}{dt} \mathbb{E}[X_6 X_7] &= \mathbb{E}[X_7^2] - \alpha_4 \mathbb{E}[X_3 X_7] \\ &\quad + \mathbb{E}[X_6 X_8] - \alpha_5 \mathbb{E}[X_3 X_6] \end{aligned}$$

$$\frac{d}{dt} \mathbb{E}[X_6 X_8] = \mathbb{E}[X_7 X_8] - \alpha_4 \mathbb{E}[X_3 X_8] - \alpha_6 \mathbb{E}[X_3 X_6]$$

$$\frac{d}{dt} \mathbb{E}[X_7^2] = 2\mathbb{E}[X_7 X_8] - 2\alpha_5 \mathbb{E}[X_3 X_7]$$

$$\frac{d}{dt} \mathbb{E}[X_7 X_8] = \mathbb{E}[X_8^2] - \alpha_5 \mathbb{E}[X_3 X_8] - \alpha_6 \mathbb{E}[X_3 X_7]$$

$$\frac{d}{dt} \mathbb{E}[X_8^2] = -2\alpha_6 \mathbb{E}[X_3 X_8]$$

Appendix 3

The detailed formula about the relations between moments and cumulants can be shown in the electronic supplementary material (ESM).

Appendix 4

In the case of using the second-order cumulant neglect closure, the stationary solutions of roll angle X_1 and roll velocity X_2 are obtained. Here, these solutions are oscillating, as shown in Fig. 11. We consider the question whether the second-order cumulant method can sufficiently reflect the nonlinearity. Therefore, we examine the effect of considering higher-order cumulants. Thus, the third-order cumulant neglect closure is used as well. Thereby, one hundred twenty third-order moment equations, derived from Eq. (24), are additionally needed. In other words, one hundred sixty-four moment equations are used in the corresponding numerical calculation. Furthermore, it is necessary that 4th and higher-order moments are represented by first, second, and third-order moments. These relations can be derived as shown in Appendix 3.

Fig. 18 shows the results when solving these moment equations numerically. Compared with the result of the second-order cumulant neglect closure in Figs. 10 and 11, it is clear that the steady state solutions are not oscillating. Furthermore, the moment values in the third-order cumulant neglect closure are closer to the moment values obtained from the numerical result of the SDE than the second-order cumulant neglect closure results, as shown in Table 7. We can therefore conclude that the result can reflect nonlinearity and be close to the actual value by using higher-order cumulants and moments.

Table 7: Moment values obtained by solving the ordinary differential equations of moment equation with third-order cumulant neglect closure method.

Item	Fn = 0.00	Fn = 0.04
$\mathbb{E}[X_1]$	0.00	0.00
$\mathbb{E}[X_1^2]$	3.66×10^{-2}	2.84×10^{-2}
$\mathbb{E}[X_2]$	0.00	0.00
$\mathbb{E}[X_2^2]$	2.37×10^{-3}	1.92×10^{-3}

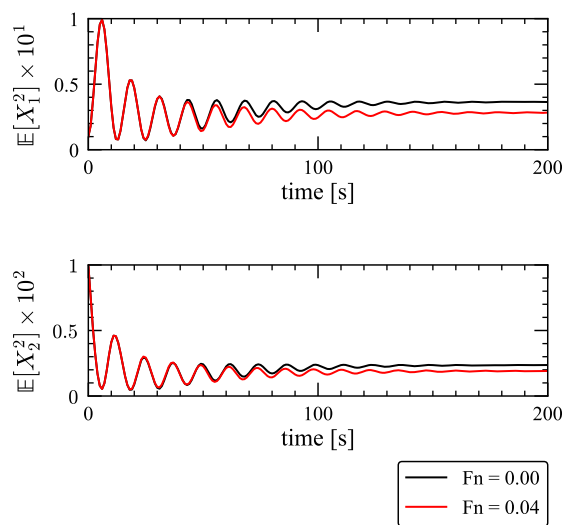


Fig. 18: Second order moment of X_1 and X_2 obtained by solving the ordinary differential equations of moment equation with third-order cumulant neglect closure method.